Theoretical Calculations on Vibrational Frequencies and Absorption Spectra of S$_1$ and S$_2$ States of Pyridine

De-Yin Wu[a,c]* (吳德印), Michitoshi Hayashi[b], Ying-Jen Shiu[a] (許瑛珍),
Kuo-Kan Liang[a] (梁國淦), Chung-Hung Chang[a] (張仲宏) and Sheng-Hsien Lin[a] (林聖賢)
[a]*Institute of Atomic and Molecular Sciences, Academia Sinica, P. O. Box 23-166, Taipei, Taiwan, 106, R.O.C.*
[b]*Center for Condensed Matter Sciences, National Taiwan University, Taipei, Taiwan, 10617, R.O.C.*
[c]*Department of Chemistry and State Key Laboratory for Physical Chemistry of Solid Surfaces,
Xiamen University, Xiamen, 361005, Fujian, P.R. China*

Three harmonic potential-energy surfaces of $^1A_1$, $^1B_1$, and $^1B_2$ singlet states of pyridine have been obtained by using *ab initio* method. Geometric properties and force fields of these states have been determined with the complete-active-space self-consistent-field (CASSCF) theoretical method. Vibrational frequencies of two excited states have been assigned on the basis of the potential energy distribution from normal mode analysis. The resulting properties are used to simulate the experimental absorption spectrum. From the spectral simulation the totally symmetric vibrations with large Huang-Rhys factors have been identified as ν_{12} and ν_{6a} modes in the $^1B_1$ state; ν_1 and ν_{12} modes in the $^1B_2$ state, indicating that these modes have strong vibronic coupling between ground and excited states.

Keywords: Pyridine; Excited state; Vibrational frequency; Vibronic coupling.

INTRODUCTION

Vibronic interactions are especially important in understanding spectroscopy and electronic structures in π-conjugated molecules. Pyridine, a model molecule, has been extensively studied by various spectroscopic techniques due to its importance in biology and medicine. For the ground state of pyridine, the structure, the dipolar moment, vibrational spectra, orbital levels, and even rovibrational spectra have been studied both experimentally and theoretically.[1-4] The results are in quite good agreement with each other. However, it is difficult to study the spectroscopic properties of the lowest two singlet excited states, $^1B_1$ (n $\rightarrow$ π*) and $^1B_2$ (π $\rightarrow$ π*). Although both transitions are optically allowed, there exist three reasons for difficulty in studying the system.[5,6] First, the absorption coefficient and the fluorescence quantum yield are extremely low for the first singlet excited state. The oscillator strength (0.003) is of the same order of magnitude as that of pyrazine and s-tetrazine, but the fluorescence quantum yield is about 6×10^{-5} and this is much lower than that of pyrazine (0.02), and that of s-tetrazine (0.001).[7-10] Second, the energy difference between $^1B_1$ and $^1B_2$ states is about 0.2-0.5 eV that is very small while the absorption spectral intensity of the $^1B_2$ state is about 10 times larger than that of the

$^1B_1$ state again.[1,5,6,11-13] This leads to the large overlap between the absorption bands of two states. Third, although the pyridine molecule in the electronic ground state prefers a planar structure with C_{2v} symmetry due to the stabilization by a strong π-delocalization, optical excitation of pyridine into the lowest excited electronic states can result in promotion of one of the valence electrons into the antibonding π* orbital.[5] Thus the pyridine ring with the planar geometry becomes destabilized and relaxes to non-planarity.[5,6,14-17] Therefore, a better understanding of the complete photophysical processes of pyridine on these low-lying states is required.

In spite of these difficulties, the absorption spectrum, fluorescence spectrum and resonance Raman spectrum have been observed in the gas phases and solutions.[7-9,11-16,18] The vibrational frequencies of a few modes of both excited states were also assigned on the basis of the experimental spectra.[1] A significant feature was found that there exist the large red shifts of some modes in the excited states. The early theoretical studies mainly concentrated on the vibronic interaction of out-of-plane modes with A_2 and B_1 symmetries.[15,19] But the strongly active vibronic modes mainly appear in the totally symmetric modes, such as ν_{6a} and ν_{12} modes for $^1B_1$, and ν_1 mode for $^1B_2$. On the other hand, the lowest excited states

---

have been studied by *ab initio* MO methods and reported in a number of papers.[2,5-7,16,20-22] These studies focused on the excitation energy and the geometry. But the reports of assignment of vibrational frequencies in both the lowest singlet states are scarce.[6,7,21] Thus, theoretical calculation should be carried out to obtain the complete fundamentals of the two excited states. The CIS/3-21G calculation gave no imaginary frequency in the S_1 state, but the previous CIS/6-31G* calculation gave one imaginary b_1 frequency, seemly indicating that the planar configuration at the $^1B_1$ state is probably a transition state under C_{2V} symmetry.[21] The stable geometry should be a boat-like configuration.[14] Recently, the result of the CAS(8,7)/6-31G** calculation showed that the C_{2V} S_1 state was stable because no imaginary frequency was obtained.[7] They found that the smallest frequency is 80 cm^{-1} that corresponds to the fundamental frequency of the ν_{16b} mode whose frequency is ~ 60 cm^{-1} from the assignment of the experimental absorption spectra.[14] They have concluded that the electronic correlation is very important for determination of the stable structure at the excited state, and the CIS method is probably insufficient in the CI expansion. More recently, Cai and Reimers performed the CAS(8,11)/cc-pVDZ calculation by considering the larger active spaces involved in $5a_1$, $4a_2$ and $2b_1$ orbitals. Indeed, the calculations of the vibrational frequencies of these two excited states indicate that both states are stable under C_{2V} symmetry at the CAS level.[6] They simulated the absorption and fluorescence spectra of pyridine under the harmonic oscillator approximation to the ground- and excited-state potential energy surfaces. Although Duschinsky effect,[23] which interprets the rotation of the normal modes at the excited state with respect to the ground state, and non-Condon effect,[24,25] which interprets the coupling between the different excited states, were considered in their study, there is a large discrepancy between the experimental and theoretical spectra. Furthermore, the vibrational frequencies of the excited states are not assigned well in previous papers.

In this paper we shall report calculated results and assignments of the vibrational frequencies of two excited states on the basis of normal mode analysis. The new assignments of vibrational frequencies in the lowest singlet excited states have allowed us to simulate well the absorption spectrum of pyridine in the gas phase.

THEORETICAL DETAILS

In the Born-Oppenheimer approximation, the absorption transition rate constant $W(i \rightarrow f)$ of the electronic transi-

tion $i \rightarrow f$ can be expressed in terms of the Fermi golden rule as[25]

$$W(i \rightarrow f) = \frac{\pi}{2\hbar^2} \sum_{v,v'} P_{iv} \left| \vec{\mu}_{fv',iv} \cdot \vec{E} \right|^2 D(\omega_{fv'} - \omega_{iv} - \omega) \quad (1)$$

where $\hbar$ is the Planck constant, and P_{iv} is the Boltzmann distribution function of the initial vibrational state, v, at the initial electronic state, i, at the temperature, T. $\vec{E}$ is the time-independent amplitude of the applied laser electric field, and $\vec{\mu}_{fv',iv}$ is the transition dipole moment between the initial and final states. D is the line shape function, where $\hbar\omega_{iv}$ and $\hbar\omega_{fv'}$ correspond to the energy levels of the initial and final vibronic states and ω is the optical frequency of the excitation source.

In this work the geometric parameters were obtained, using the Gaussian 98 program,[26] by performing CASSCF calculations for the ground and two singlet excited states. The multi-configuration self-consistent-field wave function was obtained in the complete active spaces of ground and excited configurations. These contain all possible promotions within a given set of molecular orbitals, four middle π-type orbitals and one lone-paired orbital for $^1A_1$ and $^1B_1$ states. On the other hand, the active orbitals for the $^1B_2$ state include the six π-type ones. The corresponding wave functions are the linear combinations of 50 and 175 configurations for the two excited states, respectively. Geometries and vibrational frequencies were then evaluated by applying the optimization procedure and the normal mode calculation. An all-electron basis set with triple-ζ quality, 6-311G**, is used to describe the electron motions of C, N and H atoms. The polarization functions of p and d were augmented for H, C, and N atoms, respectively.

The scaled vibrational frequencies were obtained for the ground and two excited states of pyridine. After performing the normal mode calculations, we obtain the harmonic vibrational frequencies of the ground and two excited states of pyridine at the optimized geometries at the CASSCF/6-311G** level. Because the vibrational frequency has been generally overestimated from *ab initio* calculations so far,[6,7] we have carried out the scaled quantum mechanical force field (SQMF) method proposed by Pulay et al.[27,28] In this method, the normal mode analysis is performed in which the CASSCF Cartesian force constants are transformed into the internal coordinate force constants. The scaled factors of the force constants for internal coordinates are determined, first, by the scaling CASSCF force field of the pyridine ground state and then by reproducing the experimental vibrational frequencies of the ground state of pyridine using the resulting scaled force constants. In the present paper, the scaled factors

Vibrational Frequencies and Absorption Spectra

J. Chin. Chem. Soc., Vol. 50, No. 3B, 2003   **737**
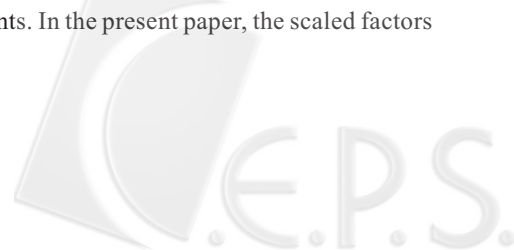
are chosen as 0.844 for C-H stretch coordinates, 0.785 for the torsion coordinates, and 0.833 for the rest of the coordinates. With these scaled factors, the experimental vibrational frequencies of the ground state of free pyridine can be reproduced well, resulting in theoretically scaled frequencies with a small deviation.[3]

For the displacements of the totally-symmetric modes with respect to the S_0 equilibrium configuration, their values are determined in terms of the transformation of the coordinates between the normal modes and the internal coordinates.[29] In this case, the normal mode Q_i can be considered to be linear combinations of the internal symmetric coordinates S_i via the matrix representation,

$$Q = L^{-1}S \qquad (2)$$

where L denotes the transformation matrix between Q and S. The S column matrix is associated with the internal coordinates through the transformation by a unitary matrix, which is 10×10 matrix for the totally-symmetric modes of pyridine in the C_{2V} point group. Thus, the displacements of these normal modes (A_1) can be calculated using

$$\Delta Q = L^{-1}U\Delta R \qquad (3)$$

where ΔR denotes a matrix of the changes of the internal coordinates at a given excited state with respect to the equilibrium geometry of the ground state. The values of ΔR elements are the differences between the geometric parameters of the excited state (S_1 or S_2) and the ground state (S_0). Here, the L matrix of the ground state was used. The equilibrium geometries of the excited and ground states are calculated as mentioned above.

When Eq. (1) is used to simulate the absorption spectra, the Franck-Condon overlap integral is computed by using the displaced-distorted harmonic oscillator model.[25] Here the totally symmetric modes all are considered to be the displaced-distorted harmonic oscillator, while the non-totally-symmetric modes are the distorted harmonic ones, which have the values of zeros of the displacements.

RESULTS AND DISCUSSIONS

0-0 Electronic Transition Energies

The positions of low-lying excited states have been determined by both experiments and high-order theoretical calculations. Experimentally, the S_1 state at 4.44 eV belongs to the n → π* transition while the S_2 state at 4.99 eV belongs to

the π → π* transition.[2] Theoretically, their transition energies previously calculated by MRD-CI, CASPT2 and SAC-CI methods are in good agreement with the experimental values.[30] In Table 1 we show excitation energies, transition dipole moments, and oscillator strengths calculated by the TD-B3LYP/6-311+G(d, p) method, together with the experimental values.[31] We can see that the observed 0-0 transition energies are clearly smaller than the TD-B3LYP energies. This is in accordance with the previous result calculated by the same method with the cc-pVDZ basis set.[6] But it is noteworthy that the transition dipole moments and oscillator strengths agree well with the experimental values.[1] As shown in Fig. 1, the bottom and upper curves correspond to potential

Table 1. 0-0 Electronic Transition Energies, Transition Dipole Moments and Oscillator Strengths of the Lowest Two Singlet States of Pyridine Molecule Calculated by TD-B3LYP/6-311+G(d,p). The Experimental Values are Listed in the Parentheses

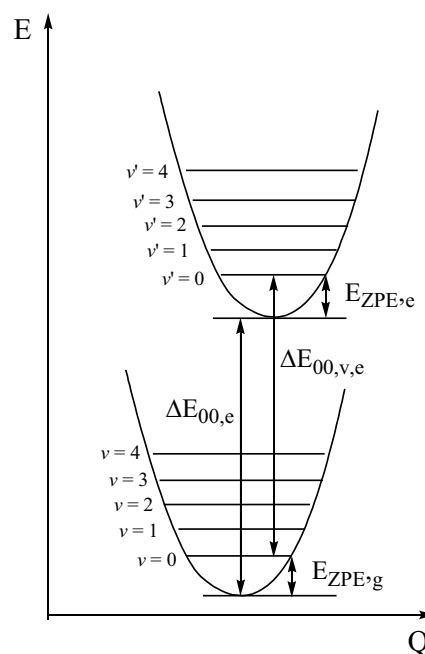| State	Excited energy (cm^{-1})	μ_e (Debye)	Oscillator strength
$^1B_1$	38549 (34771)	0.492	0.004 (0.003)
$^1B_2$	44386 (38360)	1.355	0.038 (0.04)

Fig. 1. A schematic representation of vibronic levels of a certain normal mode. The energy potential surfaces consist of two electronic states (upper: excited state; lower: ground state) and their vibrational energy levels are depicted along a given normal mode coordinate.

energy surfaces of electronic ground and excited states, respectively. $\Delta E_{00,e}$ denotes the adiabatic energy difference between the excited and ground states; $\Delta E_{00,v,e}$ is the 0-0 transition energy from the zero-point energy (ZPE) position at the ground state to that at the excited state. The energy corresponds to the experimentally observed 0-0 transition energy. $E_{ZPE,g}$ and $E_{ZPE,e}$ stand for the ZPE energies at the ground and excited states, respectively. Using these energy definitions, we can obtain the adiabatic energy differences between the excited and ground states

$$\Delta E_{00,e} = \Delta E_{00,v,e} + \left(E_{ZPE,g} - E_{ZPE,e} \right) \tag{4}$$

In Table 2 we calculated the adiabatic energy differences by considering the ZPE energy correction. The energy differences from the ZPE correction of the scaled vibrational frequencies are 4.45 and 4.92 eV for $^1B_1$ and $^1B_2$ states, respectively.[2,30] This indicates that vibrational frequencies of the excited states are predicted well at the present theoretical level, as will be seen below.

Vibrational Frequencies of Excited States

The calculated vibrational frequencies are listed in Table 3, Table 4, and Table 5. All fundamentals of the ground state of pyridine have been observed in infrared and Raman experiments.[3,4] After the SQMF procedure, the SQMF-CAS vibrational frequencies are in good agreement with the observed vibrational frequencies of the $^1A_1$ ground state.[3] But for both excited states of interests, only strongly vibronic active modes can be observed in absorption and emission experiments. For example, the vibrational bands at 60, 331, 542, 995, and 1175 cm^{-1} are assigned to ν_{16b}, ν_{10a}, ν_{6a}, ν_{12}, and ν_{9a} modes for the $^1B_1$ state;[1,6,11,14,15,18] 550, 950, and 1215 cm^{-1} are attributed to ν_{6a}, ν_1, and ν_{9a} modes for the $^1B_2$ state.[1,6] For the other vibrational modes at the two excited states, it is quite difficult to obtain their fundamentals directly from the experiment.

Comparing the vibrational frequencies of both excited states, we can see that the vibrational frequencies of some modes are very sensitive to choice of the active spaces at these two excited states. For the $^1B_1$ state, there are large differences for all A_2 modes and the ν_{15} mode with the B_2 symmetry (See Table 4). On the other hand, for the $^1B_2$ state, the large differences can be found at ν_{8a}, ν_{8b}, ν_{17a}, ν_{10a}, and ν_{16a} modes (See Table 5). Although we use the relative small active spaces for predicting the vibrational frequencies of the two excited states, the results seem reliable for the two states.

The vibrational frequencies of the $^1B_1$ state are presented in Table 4. Among four symmetric species, it is noted that some modes have not only a large shift of the vibrational frequencies but also a big change of the PED values. For A_1 modes, we provide a new assignment for the ν_{18a} mode. This is different from the assignment in the previous theoretical calculations.[6,7] The ν_{18a} mode has a clear variation on the vibrational frequency with respect to the ground state. Its vibrational frequency decreases to 802.4 cm^{-1}. We can also notice that its components of the PEDs are different significantly from those of the vibrational mode at the ground state (See Table 3). On the basis of PED values, we have assigned the unscaled vibrational frequency of 1104.1 cm^{-1} to the ν_{12} mode, which belongs to the ring symmetric bending mode. The PED value for the ν_{12} mode is 83% from the ring symmetric bending coordinate, in agreement with the PED value of 57% in the ground state. After using the SQMF procedure, we determine the ν_{12} vibrational frequency to be 1007.7 cm^{-1}. It agrees well with the experimental value of 995 cm^{-1}.[1,18] This is different from the previous studies, which assigned the unscaled vibrational frequencies (988 and 989 cm^{-1}) to this mode, respectively.[6,7] For the ν_{6a} mode, the PED value of 96% arises from the ring asymmetric bending coordinate, indicating that the normal mode is similar to the ground state. But the vibrational frequency red-shifts clearly from 600.7 cm^{-1} in the ground state to 547.8 cm^{-1} in the $^1B_1$ state. The experimental value is 542 cm^{-1}.[1,18] For the ν_1 mode, the vibrational frequencies without and with scaling are 990.7 and 904.2 cm^{-1}, respectively. There exists a large red shift com-

Table 2. The 0-0 Electronic Transition Energies (cm^{-1}) Obtained by the Zero-point Energy Correction from the Observed 0-0 Transition Energies. The Number Given in the Parenthesis is the Energy in Unit of eV

| State | E_{0-0}^{Total} [a] | E_{ZPE} | | | | ΔE_{ZPE} | ΔE_{0-0}^{E} |
		Becucci[b]	Cai[c]	CAS	SQMF		
$^1A_1$	0.0	18897.7[d]	18924.6[e]	20724.8	18883.1		
$^1B_1$	34771	19136.5	19410.0	19447.6	17728.4	-1154.7 (-0.143)	35925.7 (4.45)
$^1B_2$	38360	19387.0	19406.0	19241.0	17553.3	-1329.9 (-0.165)	39689.9 (4.92)

[a] Reference 1. [b] Reference 7. [c] Reference 6.

Table 3. Calculated Vibrational Frequencies and Potential Energy Distributions of Normal Modes at the First Singlet Excited State ($^1A_1$)

Symmetry	Expt.[a]	B3LYP[a]	CAS	SQMCAS	PED [b]	Modes
A_1	3094.2	3088.7	3359.1	3085.8	$S_5(69)$, $S_6(23)$	ν_2
	3072.8	3065.4	3331.5	3060.5	$S_6(65)$, $S_4(26)$	ν_{13}
	3030.1	3046.0	3318.3	3048.4	$S_4(68)$, $S_5(22)$, $S_6(12)$	ν_{20a}
	1583.9	1592.4	1783.3	1627.6	$S_2(52)$, $S_9(17)$, $S_1(18)$, $S_3(13)$	ν_{8a}
	1483.4	1482.0	1641.3	1498.0	$S_9(38)$, $S_{10}(33)$, $S_3(20)$, $S_1(19)$	ν_{19a}
	1218.0	1218.2	1334.0	1217.5	$S_9(41)$, $S_1(20)$, $S_{10}(18)$	ν_{9a}
	1071.9	1072.4	1171.7	1069.4	$S_{10}(34)$, $S_1(22)$, $S_3(21)$	ν_{18a}
	1031.7	1027.0	1116.8	1019.3	$S_7(57)$, $S_3(26)$, $S_2(10)$	ν_{12}
	991.4	991.3	1086.4	991.5	$S_7(33)$, $S_1(25)$, $S_2(22)$, $S_3(19)$	ν_1
	601.4	605.1	658.2	600.7	$S_8(95)$	ν_{6a}
A_2	966.0	983.8	1124.5	996.3	$S_{14}(80)$, $S_{13}(25)$, $S_{12}(23)$	ν_{17a}
	871.0	877.4	984.0	871.8	$S_{12}(69)$, $S_{14}(17)$	ν_{10a}
	373.0	374.5	433.3	383.9	$S_{13}(73)$, $S_{12}(12)$	ν_{16a}
B_1	1007.0	994.8	1127.3	998.8	$S_{16}(50)$, $S_{15}(37)$, $S_{17}(26)$, $S_{18}(12)$	ν_5
	936.6	939.4	1072.2	950.0	$S_{11}(63)$	ν_{10b}
	744.0	745.2	836.9	741.5	$S_{17}(33)$, $S_{11}(26)$, $S_{16}(26)$, $S_{15}(11)$	ν_4
	700.3	702.8	755.6	687.2	$S_{15}(45)$, $S_{17}(43)$	ν_{11}
	403.3	410.3	462.1	409.4	$S_{18}(79)$	ν_{16b}
B_2	3086.9	3081.1	3350.8	3078.2	$S_{23}(91)$	ν_{20b}
	3042.4	3043.7	3318.1	3048.2	$S_{22}(91)$	ν_{7b}
	1580.5	1586.9	1772.7	1617.9	$S_{21}(41)$, $S_{19}(27)$, $S_{27}(13)$, $S_{24}(12)$	ν_{8b}
	1441.9	1442.0	1591.3	1452.4	$S_{26}(24)$, $S_{27}(22)$, $S_{20}(21)$, $S_{25}(14)$	ν_{19b}
	1362.3	1357.9	1493.7	1363.2	$S_{25}(67)$, $S_{26}(17)$, $S_{27}(13)$	ν_{14}
	1227.0	1259.7	1297.9	1184.6	$S_{26}(44)$, $S_{19}(34)$, $S_{27}(34)$, $S_{20}(11)$	ν_3
	1143.3	1148.3	1165.6	1063.8	$S_{21}(68)$, $S_{19}(47)$, $S_{27}(15)$	ν_{15}
	1079.0	1056.0	1145.9	1045.8	$S_{20}(87)$, $S_{26}(12)$	ν_{18b}
	652.0	656.8	717.1	654.5	$S_{24}(90)$	ν_{6b}

[a] Data extracted from Reference 4. [b] Symmetric coordinates are defined as follows: S_1, C-N symmetric stretch: $(2)^{-1/2}[r(N-C_2) + r(N-C_6)]$; S_2, C-C symmetric stretch: $(2)^{-1/2}[r(C_2-C_3) + r(C_5-C_6)]$; S_3, C-C symmetric stretch: $(2)^{-1/2}[r(C_3-C_4) + r(C_5-C_4)]$; S_4, C-H symmetric stretch: $(2)^{-1/2}[r(C_2-H_7) + r(C_6-H_{11})]$; S_5, C-H symmetric stretch: $(2)^{-1/2}[r(C_3-H_8) + r(C_5-H_{10})]$; S_6, C-H stretch: $r(C_4-H_9)$; S_7, symmetric ring deformation: $(6)^{-1/2}[a(C_2-N_1-C_6) - a(N_1-C_2-C_3) - a(N_1-C_6-C_5) + a(C_2-C_3-C_4) + a(C_6-C_5-C_4) - a(C_3-C_4-C_5)]$; S_8, asymmetric ring deformation: $(12)^{-1/2}[2a(C_2-N_1-C_6) - a(N_1-C_2-C_3) - a(N_1-C_6-C_5) - a(C_2-C_3-C_4) - a(C_6-C_5-C_4) + 2a(C_3-C_4-C_5)]$; S_9, C-H in-plane bend: $(2)^{-1/2}[\beta(C_3-H_7) - \beta(C_5-H_{11})]$; S_{10}, C-H in-plane bend: $(2)^{-1/2}[\beta(C_2-H_7) - \beta(C_6-H_{11})]$; S_{11}, C-H out-of-plane bend: $(2)^{-1/2}[\gamma(C_2-H_7) - \gamma(C_6-H_{11})]$; S_{12}, C-H out-of-plane bend: $(2)^{-1/2}[\gamma(C_3-H_7) - \gamma(C_5-H_{11})]$; S_{13}, ring torsion: $(12)^{-1/2}[-\tau(N-C_2) - \tau(N-C_6) + 2\tau(C_2-C_3) + 2\tau(C_5-C_6) - \tau(C_3-C_4) - \tau(C_4-C_5)]$; S_{14}, C-H out-of-plane bend: $(2)^{-1/2}[\gamma(C_2-H_7) + \gamma(C_6-H_{11})]$; S_{15}, C-H out-of-plane bend: $(2)^{-1/2}[\gamma(C_3-H_7) + \gamma(C_5-H_{11})]$; S_{16}, C-H out-of-plane bend: $\gamma(C_4-H_9)$; S_{17}, ring torsion: $(6)^{-1/2}[\tau(N-C_2) + \tau(N-C_6) - \tau(C_2-C_3) - \tau(C_5-C_6) + \tau(C_3-C_4) + \tau(C_4-C_5)]$; S_{18}, ring torsion: $1/2[\tau(N-C_2) - \tau(N-C_6) + \tau(C_3-C_4) - \tau(C_4-C_5)]$; S_{19}, C-N asymmetric stretch: $(2)^{-1/2}[r(N-C_2) - r(N-C_6)]$; S_{20}, C-C asymmetric stretch: $(2)^{-1/2}[r(C_2-C_3) - r(C_5-C_6)]$; S_{21}, C-C asymmetric stretch: $(2)^{-1/2}[r(C_3-C_4) - r(C_5-C_4)]$; S_{22}, C-H asymmetric stretch: $(2)^{-1/2}[r(C_2-H_7) - r(C_6-H_{11})]$; S_{23}, C-H asymmetric stretch: $(2)^{-1/2}[r(C_3-H_8) - r(C_5-H_{10})]$; S_{24}, asymmetric ring deformation: $(6)^{-1/2}[a(N_1-C_2-C_3) - a(N_1-C_6-C_5) - a(C_2-C_3-C_4) + a(C_6-C_5-C_4)]$; S_{25}, C-H in-plane bend: $(2)^{-1/2}[\beta(C_3-H_7) + \beta(C_5-H_{11})]$; S_{26}, C-H in-plane bend: $(2)^{-1/2}[\beta(C_2-H_7) + \beta(C_6-H_{11})]$; S_{27}, C-H in-plane bend: $\beta(C_4-H_9)$. Here r and a denote the bond distance and bond angle, respectively. β and τ denote the in-plane bending angle and the torsion angle.

pared to the vibrational frequency (991.5 cm^{-1}) at the ground state of pyridine.[3,4]

For A_2 modes the large difference can be found in ν_{10a} and ν_{17a} modes. This kind of vibrational modes with A_2 symmetry possibly promotes strong vibronic coupling between $^1B_1$ and $^1B_2$ states.[15,19] Their vibrational frequencies depend strongly on the size of the active space and the basis sets. Becucci et al. predicted the vibrational frequencies of 902 and 562 cm^{-1} for the ν_{10a} and ν_{17a} modes whereas Cai and Reimers obtained 1465 and 820 cm^{-1}.[6,7] It is clear that the latter values are larger than our results (See Table 4). The ν_{10a} mode is thought to have strong vibronic activity. An earlier
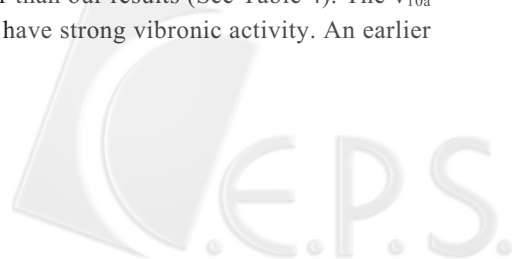
Table 4. Calculated Vibrational Frequencies and Potential Energy Distributions of Normal Modes at the First Singlet Excited State ($^1B_1$)

Symmetry	Becucci[a]	Cai[b]	CAS	SMQCAS	PED[c]	Modes
A_1	3425	3412	3398.0	3121.6	$S_4(90)$	ν_{20a}
	3394	3385	3370.9	3096.7	$S_6(85)$	ν_{13}
	3365	3354	3340.7	3069.0	$S_5(87), S_6(10)$	ν_2
	1693	1688	1676.1	1529.8	$S_2(67), S_9(25), S_1(11)$	ν_{8a}
	1537	1518	1517.2	1384.7	$S_{10}(60), S_9(30)$	ν_{19a}
	1256	1241	1256.5	1146.7	$S_9(41), S_{10}(25), S_2(23)$	ν_{9a}
	1099	1088	1104.1	1007.7	$S_7(83)$	ν_{12}
	988	989	990.7	904.2	$S_1(50), S_3(20), S_7(15)$	ν_1
	961	955	879.1	802.4	$S_3(71), S_1(30)$	ν_{18a}
	594	591	600.3	547.8	$S_8(96)$	ν_{6a}
A_2	902	1465	1003.3	889.0	$S_{13}(41), S_{12}(40), S_{14}(19)$	ν_{10a}
	562	820	755.9	669.7	$S_{14}(87), S_{12}(22)$	ν_{17a}
	428	472	475.8	421.5	$S_{13}(57), S_{12}(23)$	ν_{16a}
B_1	899	908	989.3	876.5	$S_{15}(59), S_{17}(26), S_{11}(23)$	ν_{11}
	688	709	818.6	725.3	$S_{11}(76), S_{15}(17)$	ν_{10b}
	545	544	612.7	542.9	$S_{16}(68), S_{15}(13)$	ν_5
	527	525	570.7	505.6	$S_{17}(68), S_{16}(27), S_{15}(22)$	ν_4
	80	87	126.6	112.2	$S_{18}(48), S_{17}(35), S_{16}(12)$	ν_{16b}
B_2	3419	3405	3393.1	3117.1	$S_{22}(94)$	ν_{7b}
	3366	3356	3342.2	3070.4	$S_{23}(94)$	ν_{20b}
	1633	1620	1641.7	1498.4	$S_{20}(62), S_{27}(18), S_{25}(14)$	ν_{18b}
	1471	1462	1453.4	1326.5	$S_{26}(29), S_{19}(25), S_{27}(24), S_{25}(22)$	ν_{8b}
	1420	1405	1425.9	1301.4	$S_{25}(23), S_{26}(23), S_{21}(20), S_{27}(13)$	ν_{19b}
	1321	1293	1328.5	1212.5	$S_{27}(34), S_{19}(30), S_{26}(19), S_{25}(16)$	ν_{14}
	1144	1138	1175.3	1072.7	$S_{25}(27), S_{20}(25), S_{19}(20), S_{26}(19)$	ν_3
	907	765	988.7	902.4	$S_{21}(73), S_{19}(16), S_{24}(11)$	ν_{15}
	649	625	659.8	602.1	$S_{24}(98)$	ν_{6b}

[a] From Reference 7. [b] From the supplement of Reference 6. [c] The definition is the same as that in Table 1.

study thought that the vibrational mode should have a vibrational frequency of 864 cm^{-1}.[1] Ito et al. assigned the value of 331 cm^{-1} to the rotation mode.[15] According to the PED, we assigned the mode a vibrational frequency of 889 cm^{-1}, which agrees well with the earlier assignment.[1] All calculations in the literature indicate that three vibrational frequencies are larger than 331 cm^{-1} at the $^1B_1$ state.[6,7]

For B_1 modes, all un-scaled vibrational frequencies calculated in this work are slightly larger than those calculated by Becucci et al. and Cai and Reimers.[6,7] Among the 5 modes, the vibrational frequencies of 60 and 484 cm^{-1} were observed and assigned to ν_{16b} and ν_{11} modes. Becucci et al. and Cai and Reimer obtained 80 and 87 cm^{-1} with the large active space and those values are smaller than our calculated value (126.6 cm^{-1}) because of the small active space. After using the SQMF procedure, we can obtain a scaled frequency of about 112.2 cm^{-1}. This implies that it is necessary to consider the electronic correlation for an accurate prediction of the vibrational frequency of the ν_{16b} mode. The previous studies assigned the calculated frequencies of 527 and 525 cm^{-1} corresponding to

the ν_{11} mode.[6,7] On the basis of normal mode analysis, both frequencies probably correspond to the ν_4 mode. We calculate the vibrational frequencies without and with the SQMF procedure to be 570.7 and 505.7 cm^{-1}, respectively. The latter one agrees well with the experimental value of 484 cm^{-1}. On the other hand, we assigned the ν_{11} mode with a frequency of 876.5 cm^{-1}. As mentioned above, the vibrational frequency of the ν_{15} mode depends on the size of the active space and the basis set used. We obtained the vibrational frequency of 988.7 cm^{-1}, which is larger than the values of 765 cm^{-1} predicted by Cai and Reimers and 907 cm^{-1} by Becucci et al.[6,7] A comparison of the other frequencies among B_2 modes indicates that our calculated result is almost the same as the previous results.

The selections of the active space and the basis set seem to have a small effect on the vibrational frequencies of the $^1B_2$ state except for A_2 modes. The vibrational frequencies and the PED values of various modes in the $^1B_2$ state are presented in Table 5. The exception is that the vibrational frequencies calculated by Cai and Reimers[6] are larger than our

Vibrational Frequencies and Absorption Spectra

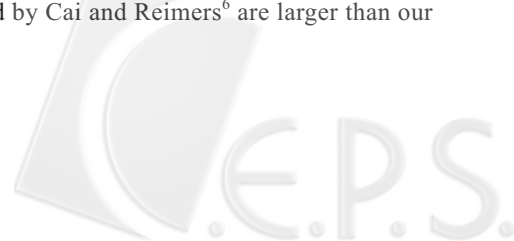*J. Chin. Chem. Soc., Vol. 50, No. 3B, 2003* **741**

Table 5. Calculated Vibrational Frequencies and Potential Energy Distributions of Normal Modes at the First Singlet Excited State ($^1B_2$)

Symmetry	Becucci[a]	Cai[b]	CAS	SMQCAS	PED[c]	Modes
A_1	3402	3395	3379.5	3071.5	$S_6(69)$, $S_5(25)$	ν_{13}
	3384	3372	3358.4	3104.6	$S_4(51)$, $S_6(25)$, $S_5(24)$	ν_{20a}
	3372	3356	3343.4	3085.3	$S_5(51)$, $S_4(43)$	ν_2
	1879	1660	1659.7	1514.8	$S_2(45)$, $S_9(22)$, $S_{10}(19)$, $S_3(11)$	ν_{8a}
	1552	1529	1540.7	1406.2	$S_9(55)$, $S_{10}(37)$	ν_{19a}
	1278	1261	1270.1	1159.2	$S_{10}(32)$, $S_9(22)$, $S_2(17)$, $S_1(14)$	ν_{9a}
	1092	1078	1087.9	992.9	$S_7(91)$	ν_{12}
	984	980	974.8	889.8	$S_3(75)$, $S_2(18)$	ν_{18a}
	978	979	970.7	885.9	$S_1(70)$, $S_2(15)$	ν_1
	565	558	562.6	513.5	$S_8(97)$	ν_{6a}
A_2	772	958	757.0	670.7	$S_{14}(69)$, $S_{13}(31)$, $S_{12}(28)$	ν_{17a}
	664	765	661.5	586.1	$S_{12}(60)$, $S_{14}(24)$	ν_{10a}
	299	327	298.8	264.7	$S_{13}(67)$, $S_{12}(16)$, $S_{14}(12)$	ν_{16a}
B_1	732	731	719.3	637.3	$S_{11}(59)$, $S_{15}(37)$, $S_{17}(21)$	ν_{10b}
	647	642	639.5	566.6	$S_{15}(47)$, $S_{11}(32)$, $S_{18}(17)$, $S_{16}(13)$	ν_{11}
	519	516	522.9	463.2	$S_{17}(39)$, $S_{16}(34)$, $S_{15}(21)$	ν_4
	485	477	484.7	429.5	$S_{16}(42)$, $S_{17}(39)$, $S_{18}(15)$	ν_5
	290	276	279.0	247.2	$S_{18}(72)$, $S_{16}(15)$	ν_{16b}
B_2	3385	3372	3360.0	3086.8	$S_{23}(69)$, $S_{22}(30)$	ν_{20b}
	3371	3356	3343.9	3072.0	$S_{22}(69)$, $S_{23}(30)$	ν_{7b}
	1673	1872	1868.8	1705.6	$S_{19}(35)$, $S_{20}(28)$, $S_{21}(23)$	ν_{8b}
	1647	1636	1633.2	1490.6	$S_{21}(46)$, $S_{19}(26)$, $S_{27}(18)$, $S_{25}(14)$	ν_{15}
	1490	1466	1479.0	1349.9	$S_{26}(49)$, $S_{27}(34)$, $S_{19}(11)$	ν_{19b}
	1456	1430	1448.5	1322.0	$S_{25}(78)$	ν_{14}
	1234	1216	1226.1	1119.1	$S_{26}(40)$, $S_{27}(39)$, $S_{21}(10)$	ν_3
	982	969	972.8	887.9	$S_{20}(64)$, $S_{21}(20)$, $S_{19}(13)$	ν_{18b}
	642	635	639.4	583.6	$S_{24}(90)$	ν_{6b}

[a] From Reference 7, these vibrational frequencies are in the same order as in Reference 7. [b] From the supplement of Reference 6. [c] The definition of the symmetric coordinates is the same as that in Table 1.

calculated frequencies and those in a previous study.[7] It is also noted that Becucci et al. gave the vibrational frequencies of the ν_{8a} and ν_{8b} modes opposite to the values of Cai and Reimers' and our calculations. If our prediction is reliable on the SQMF procedure, the vibrational frequency of the ν_{8b} mode will blue-shift to about 1706 cm^{-1}. For the $^1B_2$ state, the observed values are 550, 950, and 1215 cm^{-1} for ν_{6a}, ν_1, and ν_{9a} modes, respectively.[1] After the SQMF procedure, we determined that their vibrational frequencies are 513.5, 885.9 (889.8), 1159.2 cm^{-1}, respectively. These calculated frequencies all are smaller than the experimental values. It is probably due to the fact that we use a set of smaller scaling factors for the CASSCF force constants. Comparing the data in Tables 3 and 5, we can see that PED values for various modes in $^1B_2$ are different from those at the ground state. For example, the ν_{12} mode has a change of the PED values from 57% S_7, 26% S_3 and 10% S_2 at the ground state (See Table 3) to 91% S_7 at the excited state (See Table 5); the ν_1 and ν_{18a} modes almost all arise from the C-N stretch and the C-C stretch, re-

spectively. The ring symmetric bending coordinate does not contribute to either vibrational mode in $^1B_2$. Additionally, the vibrational frequencies of the ν_{16a} and ν_{16b} modes red-shift clearly.

Huang-Rhys Factors

Under the harmonic oscillator approximation, the Huang-Rhys factor is an important quantity, which can measure the strength of the coupling between electronic and vibrational states.[32] The relaxation energy at an excited state can be determined by the Huang-Rhys factor of the given vibrational coordinate. For each non-totally-symmetric mode the Huang-Rhys factor is zero due to the symmetry itself. In Table 6 and Table 7 we present the optimized structures of the ground and excited states and changes of internal coordinates as well as the displacements and Huang-Rhys factors of A_1 normal coordinates. We can see that for the ground state there exists a certain difference between the calculated and the experimental structures in Table 6. But it is expected that the
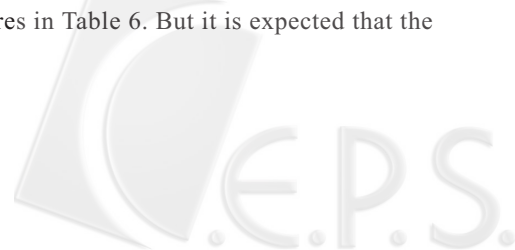
Table 6. Calculated Geometries of the S_0, S_1, S_2 States of Pyridine by Using CAS/6-311G**:
the Bond Length (angstroms) and Angles (degrees)

|	$^1A_1$	$^1B_1$	ΔR	$^1B_2$	ΔR	$^1A_1{}^a$
N_1-C_2	1.3195	1.3682	0.0487	1.3692	0.0497	1.3376
C_2-C_3	1.3845	1.3512	-0.0333	1.4327	0.0482	1.3938
C_3-C_4	1.3829	1.4325	0.0496	1.4331	0.0502	1.3916
C_2-H_7	1.0766	1.0706	-0.0060	1.0733	-0.0033	1.0857
C_3-H_8	1.0743	1.0742	-0.0001	1.0730	-0.0013	1.0818
C_4-H_9	1.0756	1.0714	-0.0042	1.0712	-0.0044	1.0811
C_2-N_1-C_6	117.92	128.16	10.24	115.93	-1.98	116.94
N_1-C_2-C_3	123.48	116.05	-7.43	124.30	0.81	123.80
C_2-C_3-C_4	118.24	120.43	2.19	119.60	1.36	118.53
C_3-C_4-C_5	118.64	118.88	0.24	116.28	-2.36	118.40
N_1-C_2-H_7	116.26	118.09	1.83	115.70	-0.55	116.03
C_3-C_2-H_7	120.26	125.86	5.60	120.00	-0.26	
C_2-C_3-H_8	120.30	118.81	-1.49	119.17	-1.13	120.12
C_4-C_3-H_8	121.46	120.76	-0.70	121.23	-0.22	
C_3-C_4-H_9	120.68	120.56	-0.12	121.86	1.18	120.80

[a] Experimental geometry is extracted from Reference 1.

Table 7. The Displacements (ΔQ), Dimensionless Displacements (Δ) and Huang-Rhys
Factors (s) of Totally-symmetric Normal Modes for S_1 and S_2 States of Pyridine

State	$^1B_1$			$^1B_2$		
modes	ΔQ	Δ	s	ΔQ	Δ	s
ν_2	-0.0085	-0.0572	0.0033	-0.0141	-0.0953	0.0091
ν_{13}	-0.0003	-0.0021	0.0000	0.0001	0.0007	0.0000
ν_{20a}	-0.0111	-0.0745	0.0056	-0.0068	-0.0455	0.0021
ν_{8a}	-0.1339	-0.6576	0.4324	-0.0221	-0.1084	0.0117
ν_{19a}	-0.0383	-0.1807	0.0327	-0.0081	-0.0382	0.0015
ν_{9a}	-0.2184	-0.9280	0.8611	-0.0592	-0.2517	0.0634
ν_{18a}	0.0472	0.1879	0.0353	0.0653	0.2600	0.0676
ν_{12}	0.3359	1.3059	1.7054	0.2344	0.9112	0.8303
ν_1	0.0027	0.0103	0.0001	0.3473	1.3317	1.7735
ν_{6a}	0.4862	1.4510	2.1055	-0.1738	-0.5188	0.2692

variations of the internal coordinates are reliable enough to assure that the displacements and Huang-Rhys factors of the normal modes are close to realistic values of the two excited states. For the $^1B_1$ state the bond angles of C-N-C and N-C-C become quite wide with respect to those in the ground state. As can be seen in Table 7, this leads to the ring bending modes of ν_{12} and ν_{6a} of the pyridine ring having the largest displacements among the A_1 modes. The result indicates that the two bending modes have the strongest vibronic activity, in line with previous experiments.[1] On the other hand, for the $^1B_2$ state the C-N and C-C bond distances all lengthen. From Table 7 it can be found that the ν_1 mode has the largest displacement as a result its Huang-Rhys factor is the largest among the A_1 modes. It is clear that the Huang-Rhys factor of the ν_{6a} mode is smaller than that of the ν_{12} mode.

Absorption Spectra

Figs. 2A and 2B shows the theoretical and experimental absorption spectra containing the contribution of the $^1B_1$ and $^1B_2$ states. The temperature is considered to be 298.15 K here. The damping constants used in the present calculation are 30 cm^{-1} and 500 cm^{-1} for both excited states $^1B_1$ and $^1B_2$, respectively. The large damping constant is associated with the fast relaxation processes. Both values of the damping constants are slightly larger than those in the recent transient absorption experiment of the pyridine molecule in solutions.[5] By using these parameters, we can see that the simulated spectrum is in quite good agreement with the experimental one.[11] The small deviation of about 0.1 eV in the center position may be due to the difference between the theoretical and experimental 0-0 electronic transition energies of the $^1B_2$ excited state. As has

Vibrational Frequencies and Absorption Spectra

J. Chin. Chem. Soc., Vol. 50, No. 3B, 2003 **743**
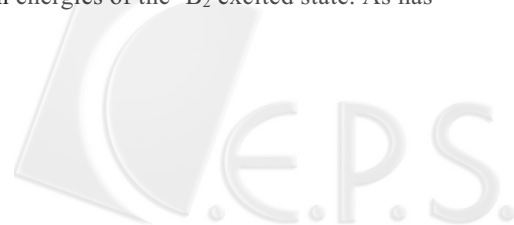
been discussed above, our calculated vibrational frequency is slightly smaller than the observed values at the $^1B_2$ excited state. Additionally, since the transition dipole moment of the $^1B_1$ state is relatively smaller than that of the $^1B_2$ state, the intensity of the $^1B_1$ state is very small and its bands largely overlap with the bands from the $^1B_2$ state (See Fig. 2B). However, due to the small damping constants and the relative long lifetime of the $^1B_1$ state, we can see a fine structure at the low energy side of the absorption spectrum from $^1B_1$. Their shapes also agree well with the experimental spectrum.

CONCLUSIONS

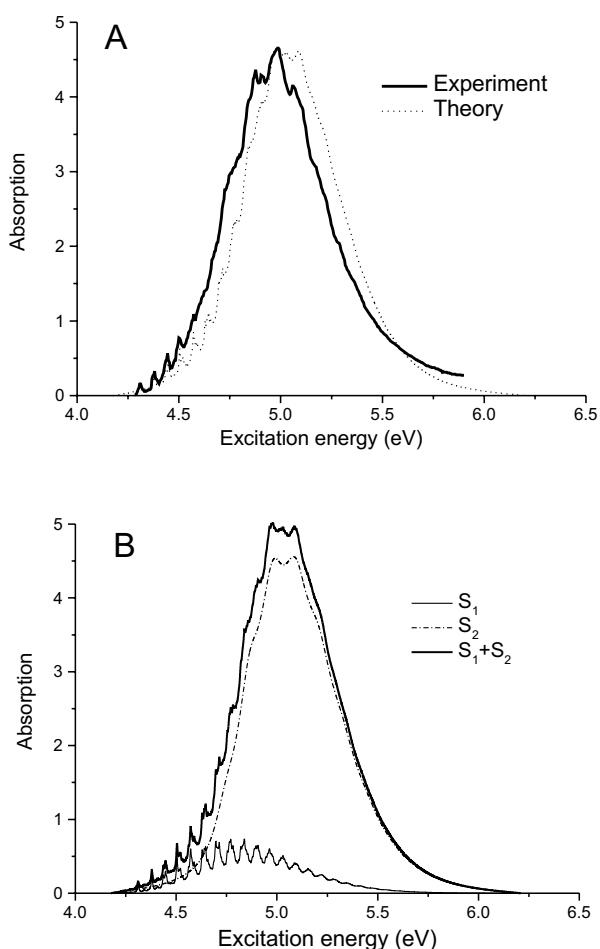We have constructed the harmonic potential-energy

Fig. 2. Theoretical absorption spectra calculated under the harmonic oscillator approximation. (A) Experimental and calculated absorption spectra; (B) Contributions of two excited states, $^1B_1$ and $^1B_2$.

surfaces of the singlet $^1A_1$, $^1B_1$, and $^1B_2$ states of pyridine by using the CASSCF method. The optimized geometries and the vibrational frequencies of the excited states have been compared with the experimental values. These equilibrium structures are used to calculate the displacements and Huang-Rhys factors of normal modes under the harmonic oscillator approximation. The fundamentals of all the vibrational modes of the two excited states have no imaginary frequency, indicating that they are stable minima under the C_{2v} symmetric point group. These vibrational frequencies of both electronic excited states have been assigned in terms of the potential energy distribution by using normal mode analysis. Due to the mixing of normal mode coordinates at the excited states, it is difficult to definitely assign the partially vibrational frequencies to the specific normal modes. However, the vibrational modes with the strong vibronic activity are clear. For example, we can assign well the calculated vibrational frequencies to the ν_{6a} and ν_{12} modes at the two excited states. In the present work, we use the same scaling factors to calculate the scaled vibrational frequencies of the two excited states. In this treatment, the scaled vibrational frequencies of the $^1B_2$ state are slightly smaller than the observed values. This causes a discrepancy between the theoretical and experimental absorption spectra. A comparison of the theoretical absorption spectrum with the experimental one indicates that under the Born-Oppenheimer approximation the displaced-distorted harmonic oscillator model is reliable in describing well the single-photon adsorption spectrum for pyridine in the gas phase.
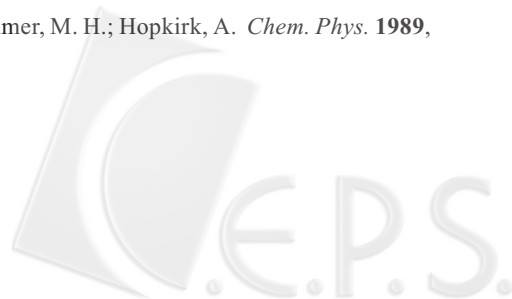
REFERENCES

1. Innes, K. K.; Ross, I. G.; Moomaw, M. R. *J. Mol. Spectrosc.* **1984**, *132*, 249.
2. Walker, I. C.; Palmer, M. H.; Hopkirk, A. *Chem. Phys.* **1989**, *141*, 365.

744 *J. Chin. Chem. Soc., Vol. 50, No. 3B, 2003*

Wu et al.

3. Klots, T. D. *Spectrochim. Acta* **1998**, *54A*, 1481.

4. Wu, D. Y.; Ren, B.; Jiang, Y. X.; Xu, X.; Tian, Z. Q. *J. Phys. Chem. A* **2002**, *106*, 9042.

5. Chachisvilis, M.; Zewail, A. H. *J. Phys. Chem. A* **1999**, *103*, 7408.

6. Cai, Z. L.; Reinmers, J. R. *J. Phys. Chem. A* **2000**, *104*, 8389.

7. Becucci, M.; Lakin, N. M.; Pietraperzia, G.; Salvi, P. R.; Castellucci, E.; Kerstel, E. R. T. *J. Chem. Phys.* **1997**, *107*, 10399 and references therein.

8. Yamazaki, I.; Baba, H. *J. Chem. Phys.* **1977**, *66*, 5826.

9. Yamazaki, I.; Murao, T.; Yoshihara, K.; Fujita, M.; Sushida, K.; Baba, H. *Chem. Phys. Lett.* **1982**, *92*, 421.

10. Meenakshi, A.; Chen, W.; Lim, E. C. *Chem. Phys. Lett.* **1988**, *148*, 507.

11. Bolovinos, A.; Tsekeris, P.; Pantos, J.; Andritsopoulos, G. *J. Mol. Spectrosc.* **1984**, *103*, 240.

12. Olsher, U.; Lubart, R.; Brith, M. *Chem. Phys.* **1976**, *17*, 237.

13. Olsher, U. *Spectrochim. Acta* **1978**, *34A*, 211.

14. Jesson, J. P.; Kroto, H. W.; Ramsay, D. A. *J. Chem. Phys.* **1972**, *56*, 6257.

15. Mochizuki, Y.; Kaya, K.; Ito, M. *J. Chem. Phys.* **1976**, *65*, 4163.

16. Zhong, D.; Diau, E. W. G.; Bernhardt, T. M.; Feyter, S. D.; Roberts, J. D.; Zewail, A. H. *Chem. Phys. Lett.* **1998**, *298*, 129.

17. Reimers, J. R. *J. Chem. Phys.* **2001**, *115*, 9103.

18. Sponer, H.; Stücklen, H. *J. Chem. Phys.* **1946**, *14*, 101.

19. Marconi, G.; Raffaelli, V. *J. Mol. Struct.* **1983**, *105*, 259.

20. Fülscher, M. P.; Andersson, K.; Roos, B. O. *J. Phys. Chem.* **1992**, *96*, 9204.

21. Foresman, J. B.; Head-Gordon, M.; Pople, J. A.; Frisch, M. J. *J. Phys. Chem.* **1992**, *96*, 135.

22. Lorentzon, L.; Fulscher, M. P.; Roos, B. O. *Theor. Chim. Acta* **1995**, *92*, 67.

23. Duschinsky, F. *Acta Physicochim. URSS* **1937**, *7*, 551.

24. Mebel, A. M.; Hayashi, M.; Lin, S. H. *Chem. Phys. Lett.* **1997**, *274*, 281.

25. Shiu, Y. J.; Hayashi, M.; Mebel, A. M.; Chen, Y.-T.; Lin, S. H. *J. Chem. Phys.* **2001**, *115*, 4080.

26. *Gaussian 98*, Frisch, M. J.; Trucks, G. W.; Schlegel, H. B.; Gill, P. M. W.; Johnson, B. G.; Robb, M. A.; Cheeseman, J. R.; Keith, T. A.; Petersson, G. A.; Montgomery, J. A.; Raghavachari, K.; Al-Laham, M. A.; Zakrzewski, V. G.; Ortiz, J. V.; Foresman, J. B.; Cioslowski, J.; Stefanov, B. B.; Nanayakkara, A.; Challacombe, M.; Peng, C. Y.; Ayala, P. Y.; Chen, W.; Wong, M. W.; Andres, J. L.; Replogle, E. S.; Gomperts, R.; Martin, R. L.; Fox, D. J.; Binkley, J. S.; Defrees, D. J.; Baker, J.; Stewart, J. P.; Head-Gordon, M.; Gonzales, C.; Pople, J. A. Gaussian Inc.: Pittsburgh, PA, 1998.

27. Pulay, P.; Fogarasi, G.; Pang, F.; Boggs, J. E. *J. Am. Chem. Soc.* **1979***, 101*, 2550.

28. Xue, Y.; Xie, D.; Yan, G. *Int. J. Quant. Chem.* **2000**, *76*, 686.

29. Califano, S. *Vibrational States*; John Wiley & Sons: London, 1976.

30. Wan, J.; Hada, M.; Ehara, M.; Nakatsuji, H. *J. Chem. Phys.* **2001**, *114*, 5117.

31. Wu, D. Y.; Hayashi, M.; Chang, C. H.; Liang, K. K.; Lin, S. H. *J. Chem. Phys.* **2003**, *118*, 4073.

32. Liao, D. W.; Mebel, A. M.; Hayashi, M.; Shiu, Y. J.; Chen, Y. T.; Lin, S. H. *J. Chem. Phys.* **1999**, *111*, 205.